Progress In Electromagnetics Research C, Vol. 121, 255–264, 2022

A New Unterminating Method for De-Embedding the Coaxial to Waveguide Transitions

Stefan Simion*

Abstract—A new unterminating method for coaxial to waveguide transitions is presented. The coaxial to waveguide transitions are modelled, and the $ABCD$ matrices of the transitions are obtained. The measured scattering parameters for the thru and short-circuit calibration standards match well the simulated scattering parameters computed from the $ABCD$ matrices. To complete the validation of the proposed unterminating method, this method is applied to the measurement of complex relative permittivity for three different dielectric materials, by using the Nicolson-Ross-Weir (NRW) transmission/reflection method. The dielectric samples are inserted one by one into a waveguide section, which is connected between two coaxial to waveguide transitions. The two transitions are de-embedded from the measured scattering parameters of the embedded waveguide section, by using the method proposed in this paper. The values obtained for the complex relative permittivity are in good agreement with those reported by other authors, for all three dielectric materials. The results presented in this paper were obtained for a frequency band ranging from 25 to 40 GHz.

1. INTRODUCTION

Because Vector Network Analyzers (VNAs) use coaxial connectors, transitions from coaxial to microstrip lines and waveguides, as well as from coaxial to the circuit pads used for on-wafer measurements, have been analyzed and used in practice (see for example [1–6] and [7–9], respectively). In all cases, VNA measures the scattering (S-) parameters of the embedded device under test. To obtain S-parameters of the device under test, the intervening transitions must be de-embedded from the S-parameters measured at the VNA reference ports. To do this, the frequency behavior of the transitions must be analyzed experimentally, this process being known as unterminating [10, 11]. Based on the measurements performed for different calibration standards, two-port parameters of the transitions can be determined [6–14].

Referring to the commercial coaxial to waveguide transitions, these are microwave components that are used as the only way to connect waveguide devices to the VNA reference ports. If the waveguide calibration standards are not available for VNA calibration at the waveguide ports, the coaxial to waveguide transition must be de-embedded, so that an unterminating technique must be used. An algorithm which minimizes the errors between the measured and simulated S-parameters for different standards has been proposed in [6] as an unterminating technique for such a transition. The method used in this work is accurate, but laborious and time consuming.

In this paper, a new noniterative unterminating technique for the coaxial to waveguide transition is proposed. It is based on the S-parameters obtained by only two measurements, performed for thru and short-circuit calibration standards, without assuming that the transitions connected to the VNA reference ports are identical. Based on the proposed method, the $ABCD$ matrices of the transitions are obtained.

Received 31 May 2022, Accepted 14 July 2022, Scheduled 27 July 2022
* Corresponding author: Stefan Simion (stefan.simion@yahoo.com).
The author is with the Department of Electronics and Communications Engineering, MTA, Bucharest 050141, Romania.

The unterminating method is validated in two steps. The first step is to compare the measured S-parameters for the thru and short-circuit standards with the simulated ones obtained from the $ABCD$ matrices of the transitions. In the second step of the validation of the unterminating method, the complex relative permittivity values for different dielectric materials are determinated using the Nicolson-Ross-Weir (NRW) method [15, 16] for a waveguide test configuration and compared to the values reported by other authors. The NRW method is commonly used for coaxial test fixture configurations [15–22], where de-embedding process is not required. Compared to the coaxial test fixture, the dielectric sample can be inserted or removed more easily, and the air gap around the sample can be greatly reduced in the case of waveguide configuration. ABS (acrylonitrile butadiene styrene), PLA (polylactic acid), and PTFE (polytetrafluoroethylene) materials were used to realize the dielectric samples for which their complex relative permittivities are determined in this paper.

The paper is organized as follows. In Section 2, the unterminating method proposed for the coaxial to waveguide transitions is described in detail. In Section 3, the measured scattering parameters are compared with those obtained from the $ABCD$ matrices of the transitions, which are developed in this paper. The proposed unterminating method is used in Section 4, where the complex relative permittivity values for three different dielectric materials are determined, and a comparison with the results reported in other papers is presented. Conclusions on the results obtained in this paper are drawn in the last section.

2. DESCRIPTION OF THE PROPOSED UNTERMINATING METHOD

The proposed unterminating method is based on two sets of measured S-parameters, which are obtained with a VNA at the coaxial ports of the coaxial to waveguide transitions. In the following, the ports of the coaxial to waveguide transitions are named Port #1 and Port #2. VNA is connected to Port #1 and Port #2 using coaxial cables, and the calibration of the VNA is performed at the ends of these coaxial cables which are connected to Port #1 and Port #2.

For the first set of measurements, the waveguide flanges of the coaxial to waveguide transitions $T1$ and $T2$ are connected directly to each other (thru standard), as shown in Fig. 1(a). The proposed equivalent circuit between ports #1 and #2 is shown in Fig. 1(b), where the input two-port circuits C_{in}, characteristic impedances Z_{c1} and Z_{c2} of the transmission lines of electrical lengths equal to 90°, as well as the electrical length θ of the transmission line of characteristic impedance Z_o, must be determined (all electrical lengths are computed at the frequency for which the equivalent circuit is determined). Also, Z_o is equal to the wave impedance on the dominant mode TE_{10} of the rectangular hollow metallic waveguides of the transitions, and its value is known as the inner width and height of the rectangular waveguides are known.

Since the measured structure is reciprocal, the scattering parameters S_{12} and S_{21} for the equivalent circuit shown in Fig. 1(b) must be equal. On the other hand, small differences between the measured S_{12} and S_{21} are observed in practice. In the following, S^{thru} is the matrix of S-parameters obtained by measurements at the coaxial ports #1 and #2 of the two-port structure shown in Fig. 1, where elements 12 and 21 are equal to each other, and equal to the square root of the product between the measured values of S_{12} and S_{21}.

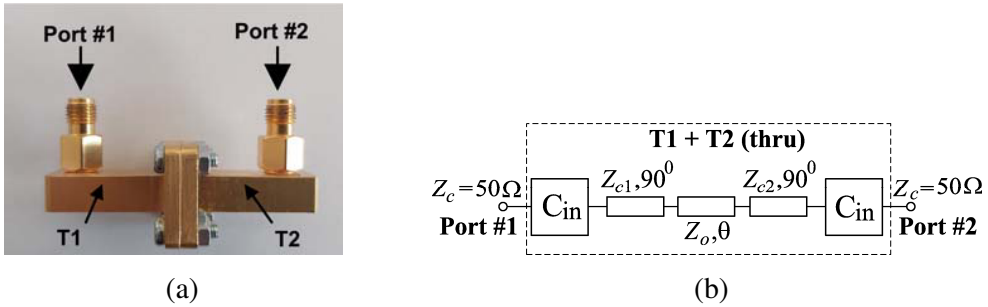

(a) (b)

Figure 1. (a) Two coaxial to waveguide transitions connected to the waveguide flanges, and (b) the proposed equivalent circuit of this structure.

The matrix S^{thru} can be transformed into the $ABCD$ matrix A^{thru}, as well as into the impedance matrix Z^{thru}. The measured structure shown in Fig. 1(a) is not lossless, such that the elements of the Z^{thru} matrix are complex numbers. Because the transmission lines used in the proposed equivalent circuits are lossless, all losses are included into the input circuits C_{in}. Here, the transitions are assumed to be identical in terms of losses. In practice, if transitions of the same type are used, the differences between their losses are really very small, so that this hypothesis can be taken into account. If Z_x is the impedance matrix of the lossless two-port consisting of the three lossless transmission lines shown in Fig. 1(b), we may impose that Z_x can be obtained by letting the real parts of the Z^{thru} matrix elements equal to zero, so that $Z_x = j\text{Im}(Z^{\text{thru}})$. On the other hand, the following expressions can be obtained analytically for the elements of the impedance matrix Z_x:

$$Z_{11} = -jZ_{c1}^2/[Z_o \tan(\theta)], \tag{1}$$

$$Z_{22} = -jZ_{c2}^2/[Z_o \tan(\theta)] \quad \text{and} \tag{2}$$

$$Z_{12} = Z_{21} = jZ_{c1}Z_{c2}/[Z_o \sin(\theta)], \tag{3}$$

with all these impedances being imaginary numbers. If $X_{11} = \text{Im}(Z_{11})$, $X_{22} = \text{Im}(Z_{22})$, and $X_{12} = \text{Im}(Z_{12})$, from (1)–(3), $\cos(\theta) = \pm(\sqrt{X_{11}X_{22}/X_{12}^2})$ is obtained.

The reactances X_{11} and X_{22} have the same signs, either positive or negative. Therefore, two cases are possible. When X_{11} and X_{22} are both negative numbers, $\theta = n \cdot \pi + \cos^{-1}(\sqrt{X_{11}X_{22}/X_{12}^2})$, while if X_{11} and X_{22} are both positive numbers, $\theta = n \cdot \pi - \cos^{-1}(\sqrt{X_{11}X_{22}/X_{12}^2})$, where n is an odd or even number, chosen such that the phase angles of the transmission S-parameters for the circuit shown in Fig. 1(b) match the values obtained by measurements.

For both cases, the characteristic impedances Z_{c1} and Z_{c2} can be derived from expressions (1) and (2), so that: $Z_{c1} = \sqrt{-Z_o X_{11} \tan(\theta)}$ and $Z_{c2} = \sqrt{-Z_o X_{22} \tan(\theta)}$.

If A_{in} is the $ABCD$ matrix of the input circuit C_{in}, this matrix can be found with Mathcad [23], as solution of the matrix equation $A^{\text{thru}} = A_{in}A_xA_{in}$, where A_x is the $ABCD$ matrix obtained from the impedance matrix Z_x.

For the second set of measurements, the waveguide flanges of the two transitions are connected to each other with a shorting metal plate inserted between them, as shown in Fig. 2(a) (short-circuit standard). For the resulting two-port structure, the reflection scattering parameters S_{11} and S_{22} at the coaxial ports #1 and #2, respectively, are measured. The equivalent circuits of the short-ended transitions $T1$ and $T2$ are presented in Figs. 2(b), (c), where θ_1 and θ_2 must be determined so that $\theta = \theta_1 + \theta_2$, while Z_s is the equivalent impedance of the shorting metal plate.

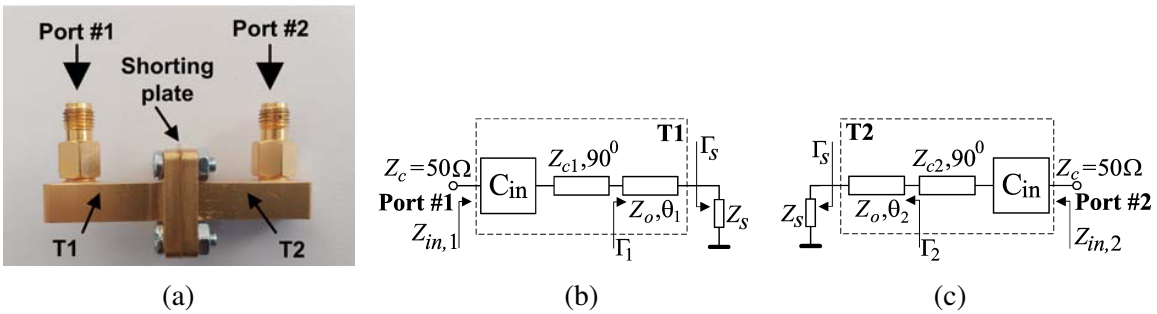

(a) (b) (c)

Figure 2. (a) Coaxial to waveguide transitions $T1$ and $T2$ short-ended at the waveguide flanges, and the proposed equivalent circuits for (b) $T1$ and (c) $T2$.

Knowing S_{11} and S_{22}, the input impedances of the two short-ended transitions can be computed using the formulas: $Z_{in,1} = Z_c(1 + S_{11})/(1 - S_{11})$ and $Z_{in,2} = Z_c(1 + S_{22})/(1 - S_{22})$, respectively (see Chapter 4 of [24]).

If the $ABCD$ matrix A_{in} is known, the characteristic impedances Z_{c1} and Z_{c2}, as well as $Z_{in,1}$ and $Z_{in,2}$, are calculated as shown before, and the values of the reflection coefficients Γ_1 and Γ_2 from Figs. 2(b), (c) can also be calculated.

In order to compute θ_1 and θ_2, from Figs. 2(b), (c), we can write: $\Gamma_1 = \Gamma_s \cdot \exp(-j2\theta_1)$ and $\Gamma_2 = \Gamma_s \cdot \exp(-j2\theta_2)$ (see Chapter 2 of [24]). Assuming $|\Gamma_1| = |\Gamma_2|$ (lossless transmission lines), it is obtained that $\theta_1 = \theta/2 + \Delta\theta/2$ and $\theta_2 = \theta/2 - \Delta\theta/2$, where $\Delta\theta = \theta_1 - \theta_2 = (\varphi_{\Gamma_2} - \varphi_{\Gamma_1})/2$, while φ_{Γ_1} and φ_{Γ_2} are the phase angles of Γ_1 and Γ_2, respectively.

The $ABCD$ matrices for the coaxial to waveguide transitions $T1$ and $T2$ can be computed as follows:

$$A_{T1} = A_{in} \cdot \begin{bmatrix} 0 & jZ_{c1} \\ j/Z_{c1} & 0 \end{bmatrix} \cdot \begin{bmatrix} \cos(\theta_1) & jZ_o \sin(\theta_1) \\ j\sin(\theta_1)/Z_o & \cos(\theta_1) \end{bmatrix} \tag{4a}$$

and

$$A_{T2} = \begin{bmatrix} \cos(\theta_2) & jZ_o \sin(\theta_2) \\ j\sin(\theta_2)/Z_o & \cos(\theta_2) \end{bmatrix} \cdot \begin{bmatrix} 0 & jZ_{c2} \\ j/Z_{c2} & 0 \end{bmatrix} \cdot A_{in} \tag{4b}$$

respectively.

Once the $ABCD$ matrices of the coaxial to waveguide transitions are known, these transitions can be de-embedded, and the $ABCD$ matrix, as well as the S-parameter matrix of the waveguide device connected between the transitions, can be found out.

3. COMPARISON BETWEEN THE EXPERIMENTAL AND SIMULATED RESULTS

The measured S-parameters for the thru and short-circuit standards were compared with the S-parameters obtained by using the matrices $ABCD$ of transitions $T1$ and $T2$, which can be determined as shown in the previous section.

In this paper, transitions from 50 Ω coaxial connector (2.92 mm — Female) to WR-28 waveguide from Pasternack are used (the inner sizes of the cross-section waveguide ports are $a = 7.111$ mm and $b = 3.556$ mm). All measurements were performed using Anritsu MS46122A-040 VNA.

For the thru setup, the magnitude and phase of the S-parameters measured at the 50 Ω coaxial ports are compared to the simulated ones that were computed from the $ABCD$ matrix obtained by multiplying A_{T1} and A_{T2} matrices given by (4a) and (4b), respectively. The results are presented in Fig. 3. Since the elements of the equivalent circuit shown in Fig. 1(b) were computed so as to match the measured S-parameters, no differences can be observed between the experimental values and those obtained for the equivalent circuit.

When the transitions $T1$ and $T2$ are short-circuited at the waveguide ports (short-circuit standard), the reflection coefficients S_{11} and S_{22} at the 50 Ω coaxial ports can also be computed from the $ABCD$ matrices (4a) and (4b), respectively. A comparison between these simulated S-parameters and those obtained from measurements is presented in Fig. 4. Differences less than 0.05 can be observed between

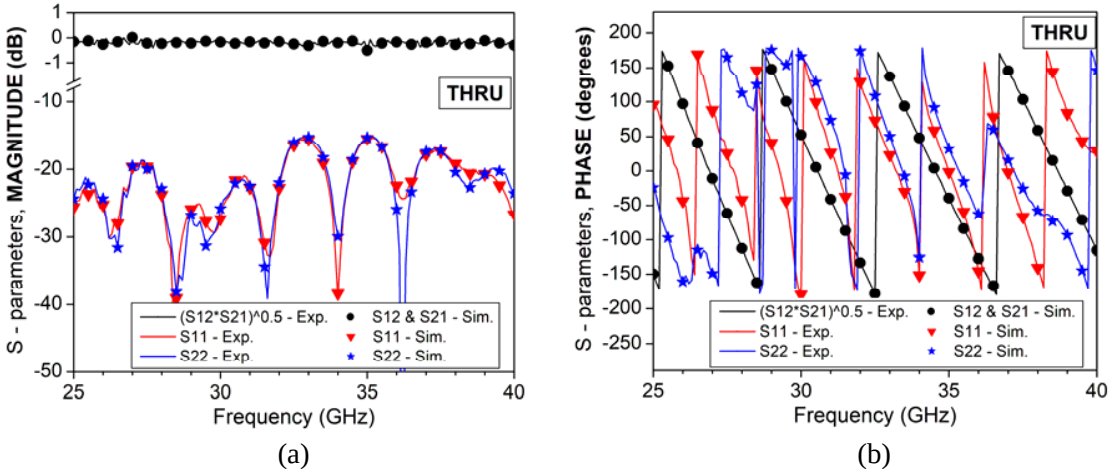

Figure 3. Measured and simulated (a) magnitude and (b) phase of the S-parameters, for the thru setup.

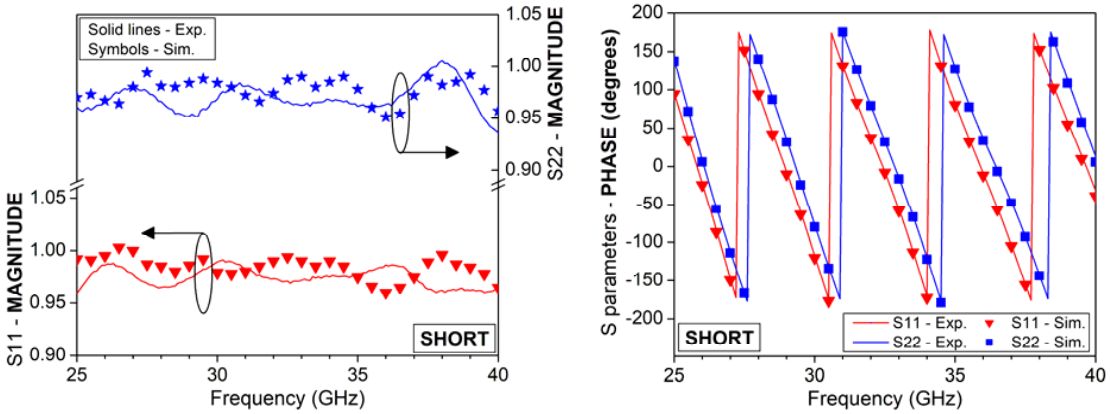

Figure 4. Measured and simulated (a) magnitude and (b) phase of the input reflection coefficients, when the waveguide ports of the coaxial to waveguide transitions are short-circuited.

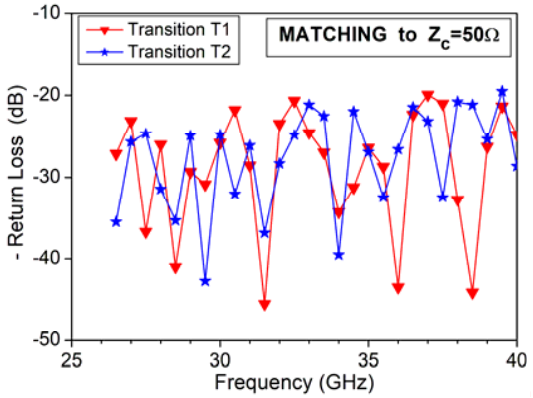

Figure 5. Simulated return-loss versus frequency computed at the 50 coaxial ports, when the waveguide ports are loaded by the wave impedance of the dominant mode TE_{10}.

the experimental and simulated magnitude values of the reflection coefficients S_{11} and S_{22}. These differences are the result of the assumption that transitions have the same losses. The differences between the simulated and experimental phase values of these reflection coefficients are less than 5 degrees.

Based on the $ABCD$ matrices determined for transitions, the return loss values at the 50 Ω coaxial ports were also computed, for the situation when the waveguide ports are loaded by the wave impedance Z_o of the dominant mode TE_{10}. The results are presented in Fig. 5. The VSWR values for both transitions are smaller than 1.25, which is the maximum value provided by the manufacturer for frequencies between 26.5 and 40 GHz.

4. APPLICATION TO THE DETERMINATION OF THE COMPLEX RELATIVE PERMITTIVITY USING THE T/R METHOD

The unterminating method presented in this paper was applied to de-embed the coaxial to waveguide transitions in an experimental setup used to determine the complex relative permittivity of three dielectric materials, by following the NRW transmission/reflection (T/R) method [15–17].

The experimental setup is presented in Fig. 6, where a rectangular metallic waveguide section (WS) of length $L_{\mathrm{WS}} = 25$ mm is inserted between two coaxial to waveguide transitions, $T1$ and $T2$. The rectangular waveguides of the transitions and WS have the same inner sizes, the width a and height b.

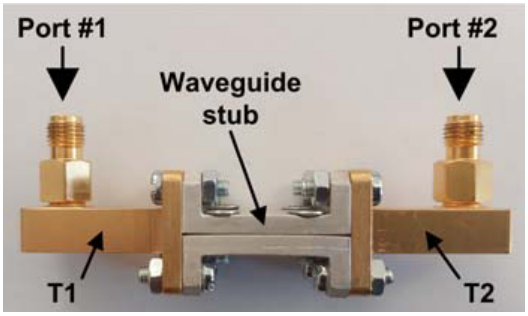

Figure 6. The waveguide measurement setup used in this paper to determine the complex relative permittivity of a dielectric sample, in order to validate the proposed unterminating method.

To use the NRW method, the scattering parameters for the hollow WS and the WS loaded with the dielectric sample must be known.

Three dielectric samples made of ABS, PLA, and PTFE materials were measured. The ABS and PLA samples were prepared by using a 3D printer. All three dielectric samples have rectangular cross-sections of width a and height b.

The relative uncertainty in complex relative permittivity due to the uncertainty of the measured scattering parameters has low values if the ratio between the sample length and the guided wavelength in the sample is greater than 1 [17]. Taking into account this design condition, the length L for each sample was chosen to be equal to 15 mm.

The measured scattering matrices at ports #1 and #2 with and without dielectric sample were transformed into the $ABCD$ matrices A_1 and A_2, respectively. Thus, if A_{T1} and A_{T2} are computed with (4a) and (4b), the $ABCD$ matrices of the WS with and without dielectric sample can be found out as $A^x = A_{T1}^{-1} \cdot A_1 \cdot A_{T2}^{-1}$ and $A^y = A_{T1}^{-1} \cdot A_2 \cdot A_{T2}^{-1}$, respectively. Finally, the scattering parameter of the WS with and without dielectric sample, S^x and S^y, respectively, can be find out (see Chapter 4 of [24]).

Combining Equations (8)–(11) and (16) given in [17], the real and imaginary parts of the complex relative permittivity of the dielectric sample, $\varepsilon_r = \varepsilon_r^{/} - j\varepsilon_r^{//}$, can be expressed as:

$$\varepsilon_r^{/} = \left(\frac{c_0}{2\pi f}\right)^2 \cdot \left\{\left(\frac{\pi}{a}\right)^2 - [\mathrm{Re}(\gamma)]^2 + [\mathrm{Im}(\gamma)]^2\right\} \quad \text{and} \quad \varepsilon_r^{//} = -2\mathrm{Re}(\gamma)\mathrm{Im}(\gamma)\left(\frac{c_0}{2\pi f}\right)^2,$$

where γ is the propagation constant in the dielectric sample, a complex number with the real and imaginary parts given by $\mathrm{Re}(\gamma) = -\ln|z|/L$ and $\mathrm{Im}(\gamma) = -(\varphi_z - 2m\pi)/L$, respectively, while φ_z is the phase angle of the complex number z, and m is an integer positive number chosen so that the function $\mathrm{Im}(\gamma)$ is continuous versus the frequency.

The complex number z is the solution of the following second order equation, for which $\mathrm{Re}(\gamma) > 0$:

$$z^2 - z \cdot \frac{S_{21}^y}{S_{21}^x}\left\{1 + (S_{12}^x S_{21}^x - S_{11}^x S_{22}^x)\exp\left[2\gamma_0(L_{\mathrm{WS}} - L)\right]\right\} \cdot \exp(\gamma_0 L) + 1 = 0,$$

where S_{ij}^x and S_{ij}^y (i and j are equal to 1 or 2) are the ij elements of the matrices S^x and S^y, respectively, while $\gamma_0 = j\sqrt{(2\pi f/c_0)^2 - (\pi/a)^2}$ is the propagation constant into the hollow WS, f the frequency, and c_0 the speed of light.

The numerical results obtained for the real and imaginary parts of the complex relative permittivity are presented in Fig. 7. In this figure, the solid lines represent the average values obtained for these parameters, for each material. The variation of the real part of ε_r versus the frequency is within ± 0.06 around the average value, for each material. On the other hand, the values obtained for the imaginary part of ε_r show large differences around the average values.

The sources of errors in the determination of ε_r are due to the uncertainty in the measured scattering parameters at the VNA coaxial reference ports and de-embedding process of the coaxial to waveguide transitions. Both sources of errors contribute to the uncertainty in the scattering parameters that are

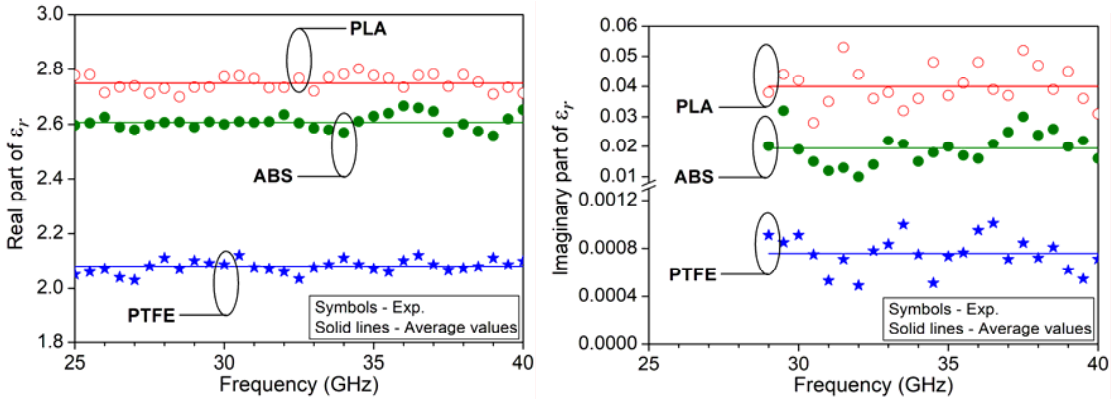

Figure 7. (a) Real part and (b) imaginary part of the complex relative permittivity versus the frequency, for ABS, PLA and PTFE materials measured in this paper by using the NRW method and the proposed unterminated method for de-embedding the coaxial to waveguide transitions.

obtained at the waveguide ports after de-embedding the coaxial to waveguide transitions. A detailed analysis of the uncertainty of ε_r in the scattering parameters by taking into account the intervening transitions is beyond the scope of this paper, but a short uncertainty analysis to explain the dispersion of the measured real and imaginary parts of ε_r around the average values is presented as follows.

The relative uncertainty in ε_r due to the measured transmission and reflection scattering parameters at the waveguide ports can be preliminarily evaluated using the relationships presented in [17], for the measurement uncertainties of the VNA at the coaxial ports. The effect of the unterminating errors could be evaluated by overestimating the measurement uncertainties of the VNA. In this way, it was observed that the uncertainties in the scattering parameters has an important effect on the imaginary part of ε_r

Table 1. Comparison with results reported by other authors for the complex relative permittivity of the ABS, PLA and PTFE materials.

	Ref.	$\varepsilon_r^{/}$	$\varepsilon_r^{//}$	Frequency range	Experimental Method
ABS	[19]	2.6	0.014	1–10 GHz	T/R, coaxial
	[20]	2.4	0.013	30–50 GHz	T/R, coaxial
	[21]	2.57	0.035	8.2–11 GHz	T/R, waveguide
	[22]	2.6	–	12–18 GHz	T/R, waveguide
		2.57	0.012	14.83 GHz	Cavity perturbation
	[25]	2.75	0.019	$\sim$ 11 GHz	Dielectric resonator
	This work	2.61	0.019	25–40 GHz	T/R, waveguide
PLA	[19]	2.71	0.017	1–10 GHz	T/R, coaxial
	[20]	2.57	0.024	30–50 GHz	T/R, coaxial
	[26]	2.75	0.033	40 GHz	R, waveguide
	[27]	2.75	0.041	2–18 GHz	T/R, coaxial
	This work	2.75	0.04	25–40 GHz	T/R, waveguide
PTFE	[20]	2.03	0.00061	30–50 GHz	T/R, coaxial
	[28]	2.08	0.0006	19.82 GHz	Resonant waveguide
	[29]	2.071	0.00097	60.291 GHz	Open resonator
	This work	2.078	0.00076	25–40 GHz	T/R, waveguide

and a small effect on the real part of ε_r. Numerical results showed that the relative uncertainty due to the transmission and reflection scattering parameters is smaller than 10^{-2} for the real part of ε_r, so that the uncertainty in the real part of ε_r is small compared to its average value. This could explain why the measured values of the real part of ε_r are closed to the average values. In contrast, the relative uncertainty in the imaginary part of ε_r due to the scattering parameters is higher ($\sim$ 0.1–1), so that any increase of the uncertainty in the scattering parameters at the waveguide ports due to the errors of the unterminating technique has a significant effect on the imaginary part value of ε_r. For example, increasing the uncertainty in the magnitude of the reflection coefficients by 0.05, the uncertainties in the imaginary part value of ε_r could be comparable to the average value, for all three materials.

A comparison between the average values obtained in this paper for the real and imaginary parts of ε_r and those reported in other references is presented in Table 1, for all three materials. As observed, the average values of both real and imaginary parts of ε_r are similar to the values measured by other authors, for all materials analyzed in this paper.

5. CONCLUSION

A simple noniterative unterminating method is proposed for the coaxial to waveguide transition. This method consists of only two measurements of scattering parameters, both performed by using a VNA connected to the coaxial ports of the transitions. Based on this method, the $ABCD$ matrices of the coaxial to waveguide transitions have been obtained. The proposed unterminating method was validated in two steps. Firstly, the measured scattering parameters for the thru and short-circuit standards were compared with the simulated scattering parameters obtained from the $ABCD$ matrices of the transitions. No differences between the experimental and simulated scatterings has been observed for the thru standard. For the short-circuit standard, some differences occur for the magnitudes of the input reflection coefficients, while the differences between the experimental and simulated phase values of these reflection coefficients are very small.

To complete the validation of the proposed unterminating method, the complex relative permittivity using the NRW method for a waveguide measurement setup was determined for three dielectric materials, and the results were compared with those reported in other references. For this task, first of all, the coaxial to waveguide transitions were de-embedded by using the $ABCD$ matrices of the transitions found in this paper. The average values obtained for the real and imaginary parts of the complex relative permittivity are in good agreement with those reported by other authors, for all three dielectric materials.

The experiments were performed in the 25–40 GHz frequency band using commercial coaxial to waveguide transitions, but the proposed unterminating method can also be used in any other frequency band.

REFERENCES

1. Majewski, M. L., R. W. Rose, and J. R. Scott, "Modeling and characterization of microstrip-to-coaxial transitions," *IEEE Trans. Microw. Theory Tech.*, Vol. 29, No. 8, 799–805, Aug. 1981, doi: 10.1109/TMTT.1981.1130450.
2. Capsalis, C., C. P. Chronopoulous, and N. K. Uzunoglu, "A rigorous analysis of a coaxial to shielded microstrip line transition," *IEEE Trans. Microw. Theory Tech.*, Vol. 37, No. 7, 1091–1098, Jul. 1989, doi: 10.1109/22.24553.
3. Hajian, M., D. P. Tran, and L. P. Ligthart, "Modeling the transition between a coaxial line and a flat rectangular waveguide," *Proc. Int. Conf. on Antennas and Propagation (ICAP'95)*, 269–272, Eindhoven, Netherlands, Apr. 4–7, 1995, doi: 10.1049/cp:19950307.
4. Liang, J.-F., H.-C. Chang, and K. A. Zaki, "Coaxial probe modeling in waveguides and cavities," *IEEE Trans. Microw. Theory Tech.*, Vol. 40, No. 12, 2172–2180, Dec. 1992, doi: 10.1109/22.179878.
5. Yao, H.-W. and K. A. Zaki, "Modeling of generalized coaxial probes in rectangular waveguides," *IEEE Trans. Microw. Theory Tech.*, Vol. 43, No. 12, 2805–2811, Dec. 1995, doi: 10.1109/22.475638.

6. Lozano-Guerrero, A. J., F. J. Clemente-Fernandez, J. Monzo-Cabrera, J. L. Pedreno-Molina, and A. Diaz-Morcillo, "Precise evaluation of coaxial to waveguide transitions by means of inverse techniques," *IEEE Trans. Microw. Theory Tech.*, Vol. 58, No. 1, 229–235, Jan. 2010, doi: 10.1109/TMTT.2009.2036408.
7. Cho, H. and D. E. Burk, "A three-step method for the de-embedding of high-frequency S-parameter measurements," *IEEE Trans. Electron Devices*, Vol. 38, No. 6, 1371–1375, Jun. 1991, doi: 10.1109/16.81628.
8. Ito, H. and K. Masuy, "A simple through-only de-embedding method for on-wafer S-parameter measurements up to 110 GHz," *Proc. IEEE MTT-S Int. Microw. Symp. Dig.*, 383–386, Atlanta, GA, USA, Jun. 15–20, 2008, doi: 10.1109/MWSYM.2008.4633183.
9. Li, X., Y. Zhang, O. Li, T. Ren, F. Guo, H. Lu, and R. Xu, "A thru-halfthru-short de-embedding method for millimeter-wave on-wafer HBT characterization," *IEEE Trans. Electron Device Lett.*, Vol. 38, No. 6, 720–723, Jun. 2017, doi: 10.1109/LED.2017.2693439.
10. Bauer, R. and P. Penfield, Jr., "De-embedding and unterminating," *IEEE Trans. Microw. Theory Tech.*, Vol. 22, No. 3, 282–288, Mar. 1974, doi: 10.1109/TMTT.1974.1128212.
11. Williams, D., "De-embedding and unterminating microwave fixtures with nonlinear least squares," *IEEE Trans. Microw. Theory Tech.*, Vol. 38, No. 6, 787–791, Jun. 1990, doi: 10.1109/22.130977.
12. Rautio, J. C., "De-embedding algorithm for electromagnetics," *Int. J. Microw. Millim.-Wave Computer-Aided Eng.*, Vol. 1, No. 3, 282–287, Mar. 1991, doi: 10.1002/mmce.4570010306.
13. Amakawa, S., K. Takano, K. Katayama, T. Yoshida, and M. Fujishima, "On the choice of cascade de-embedding methods for on-wafer S-parameter measurement," *Proc. IEEE Int. Symp. Radio-Frequency Integration Technol. (RFIT)*, 134–136, Singapore, Nov. 21–23, 2012, doi: 10.1109/RFIT.2012.6401638.
14. Wang, W., R. Jin, T. S. Bird, X. Liang, and J. Geng, "De-embedding based on EM simulation and measurement: A hybrid method," *IEEE Trans. Microw. Theory Tech.*, Vol. 65, No. 12, 5019–5034, Dec. 2017, doi: 10.1109/TMTT.2017.2715326.
15. Nicolson, A. M. and G. F. Ross, "Measurement of the intrinsic properties of materials by time-domain techniques," *IEEE Trans. Instrum. Meas.*, Vol. 19, No. 4, 377–382, Nov. 1970, doi: 10.1109/TIM.1970.4313932.
16. Weir, W. B., "Automatic measurement of complex dielectric constant and permeability at microwave frequencies," *Proc. IEEE*, Vol. 62, No. 1, 33–36, Jan. 1974, doi: 10.1109/PROC.1974.9382.
17. Jarvis, J. B., E. J. Vanzura, and W. A. Kissick, "Improved technique for determining complex permittivity with the transmission/reflection method," *IEEE Trans. Microw. Theory Tech.*, Vol. 38, No. 8, 1096–1103, Aug. 1990, doi: 10.1109/22.57336.
18. Boughriet, A. H., C. Legranf, and A. Chapoton, "Noniterative stable transmission/reflection method for low-loss material complex permittivity determination," *IEEE Trans. Microw. Theory Tech.*, Vol. 45, No. 1, 52–57, Jan. 1997, doi: 10.1109/22.552032.
19. Zechmeister, J. and J. Lacik, "Complex relative permittivity measurement of selected 3D-printed materials up to 10 GHz," *Proc. Conf. Microw. Techniques (COMITE)*, Pardubice, Czech Republic, Apr. 16–18, 2019, doi: 10.1109/COMITE.2019.8733590.
20. Reyes, N., F. Casado, V. Tapia, C. Jarufe, R. Finger, and L. Bronfman, "Complex dielectric permittivity of engineering and 3D-printing polymers at Q-band," *J. Infrared, Millim. Terahertz Waves*, Vol. 39, 1140–1147, 2018, doi: 10.1007/s10762-018-0528-9.
21. Deffenbaugh, P. I., R. C. Rumpf, and K. H. Church, "Broadband microwave frequency characterization of 3-D printed materials," *IEEE Trans. Compon. Packaging Manuf. Technol.*, Vol. 3, No. 12, 2147–2155, Dec. 2013, doi: 10.1109/TCPMT.2013.2273306.
22. Castles, F., D. Isakov, A. Lui, Q. Lei, C. E. J. Dancer, Y. Wang, J. M. Janurudin, S. C. Speller, C. R. M. Grovenor, and P. S. Grant, "Microwave dielectric characterization of 3D-printed $BaTiO_3$/ABS polymer composites," *Scientific Reports*, Vol. 6, 2016, Art. no. 22714, doi: 10.1038/srep22714.
23. *Mathcad — User's guide* (MathSoft, Inc.).

24. Pozar, D. M., *Microwave Engineering*, 4th Edition, John Wiley & Sons, 2012.
25. Riddle, B., J. B. Jarvis, and J. Krupka, "Complex permittivity measurements of common plastics over variable temperatures," *IEEE Trans. Microw. Theory Tech.*, Vol. 51, No. 3, 727–733, Mar. 2003, doi: 10.1109/TMTT.2003.808730.
26. Felicio, J. M., C. A. Fernandes, and J. R. Costa, "Complex permittivity and anisotropy measurement of 3D-printed PLA at microwaves and millimeter-waves," *Proc. IEEE Int. Conf. on Applied Electromagnetics and Communications (ICECOM)*, Dubrovnik, Croatia, Sept. 19–21, 2016, doi: 10.1109/ICECom.2016.7843900.
27. Elsallal, M. W., J. Hood, I. McMichael, and T. Busbee, "3D printed material characterization for complex phased arrays and metamaterials," *Microw. J.*, Vol. 59, No. 10, 20–34, 2016.
28. Rajab, K. Z., K. F. Fuh, R. Mittra, and M. Lanagan, "Dielectric property measurement using a resonant nonradiative dielectric waveguide structure," *IEEE Microw. Wirel. Compon. Lett.*, Vol. 15, No. 2, 104–106, Feb. 2005, doi: 10.1109/LMWC.2004.842845.
29. Suzuki, H. and T. Kamijo, "Millimeter-wave measurement of complex permittivity by perturbation method using open resonator," *IEEE Trans. Instrum. Meas.*, Vol. 57, No. 12, 2868–2873, Dec. 2008, doi: 10.1109/TIM.2008.926448.